



Analytical study of the aerodynamic noise emitted by distributed electric propulsion systems

Daniel Acevedo-Giraldo*, Michel Roger[†] and Marc C. Jacob[‡]

Univ Lyon, École Centrale de Lyon, CNRS, Univ Claude Bernard Lyon 1, INSA Lyon, LMFA, UMR 5509, 69130, Écully, France

Hadrien Bériot[§]

Siemens Industry Software, Simulation and Test Solutions, Interleuvenlaan 68, B-3001, Heverlee, Belgium

The present work addresses the installation effects expected for the tonal noise of a pair of side-by-side contrarotating subsonic propellers mounted near a wing trailing edge. This generic configuration mimics future urban air-vehicle architectures. The installation effects refer to the additional sources of aerodynamic noise caused by blade-wing interaction and their scattering by the wing, compared to the case of isolated propellers. The paper aims to demonstrate the ability of analytical models to estimate these effects, which is of primary interest for the preliminary design steps of an installed propulsion system. Furthermore, the analytical parametric study might help determine promising configurations for future aircraft. In the analytical formulation, dipole-like noise sources of the propellers are considered, assuming rigid blades. The sound radiation from the propellers is formulated in three dimensions for characteristic spinning modes of the tonal noise. In contrast, the half-plane Green's function accounts for the sound scattering by the wing. A finite-chord correction is applied to the half-plane formulation and validated by numerical simulations. The results show that the installation effect is crucial for analyzing tonal propeller noise at low frequencies. In particular, sound radiation is significantly increased when the blade tips operate in the close vicinity of the trailing edge.

I. Nomenclature

α	=	Angle of attack
α_d	=	Dipole angle
β	=	Compressibility parameter
γ	=	Blade sweep angle
ρ_0	=	Fluid density
θ, θ_0	=	Observer and source angles
ω, Ω	=	Angular frequency
τ	=	Half-time span of a Gaussian pulse
B	=	Number of blades
b_0	=	Half-width of a Gaussian distortion
C	=	Amplitude factor
c	=	Blade chord
c_0	=	Sound speed
C_L	=	Lift coefficient
F_t, F_d	=	Dipole strength and amplitude
F_s	=	Blade-loading harmonic
$G_{1/2}^{(0)}$	=	Half-plane Green's functions without flow
$G_{1/2}^{(M_0)}$	=	Half-plane Green's functions with flow

*Phd candidate, Laboratoire de Mécanique des Fluides et d'Acoustique, École Centrale de Lyon, daniel.acevedo-giraldo@ec-lyon.fr

[†]Professor, Laboratoire de Mécanique des Fluides et d'Acoustique, Ecole Centrale de Lyon, michel.roger@ec-lyon.fr, AIAA Member

[‡]Professor, Laboratoire de Mécanique des Fluides et d'Acoustique, École Centrale de Lyon, marc.jacob@ec-lyon.fr, AIAA Member

[§]Senior Research Engineering Manager, Siemens Industry Software, hadrien.beriot@siemens.com

K, k	=	Corrected and normal wavenumber
K	=	Modified Bessel function
M_0	=	Mach number
m	=	Blade-passing frequency order
n	=	Mode order
r	=	Blade radius
r, r_o	=	Observer and source radial positions
\bar{r}	=	Distance between the observer and source
R	=	Distance variables in GF
s	=	Blade-loading harmonic order
T	=	Period of rotation
t	=	Time
U_0	=	Flow velocity
u_0, u_1	=	Upper bounds of the integrals in GF
W_0	=	Instantaneous relative speed on a blade
$w(t)$	=	Periodicity of a Gaussian variation
w_0	=	Depth of wake- velocity deficit
w_s	=	Distortion harmonics
x, x_0	=	Observer and source streamwise positions
z, z_0	=	Observer and source positions

II. Introduction

IN parallel to the continuing growth of civil air transport, innovative electric and hybrid-electric aircraft concepts are presently under increasing development to meet future noise and gas emission requirements. Similarly, new flying architectures emerge at a smaller scale, from drones to urban air vehicles. All are disruptive technologies for which the airframe and the propulsion systems can no longer be optimized separately, unlike what was done in the past for the more conventional fuselage-and-wing aircraft.

A particular interest is given the Urban Air Mobility (UAM), for which many concepts emerged that are likely to lead to new sources of community noise [1–5]. These small vehicles will probably be the first to reach maturity in the near future. Related to this is the propulsion concept referred to as Distributed Electric Propulsion (DEP), relying on multiple fans or propellers installed spanwise along a wing, either as pusher or puller units. Apart from electric power-supply issues, the main challenges inherent to DEP systems include the effects of inflow distortions on propeller efficiency and noise. These effects, of aerodynamic and acoustic nature, will highly depend on the relative positioning of the propellers on the wing/airframe. The aerodynamic installation effect refers to the interaction of a propeller with mean-flow gradients around the wing, which induces additional sources of aerodynamic noise. The acoustic installation effect refers to the scattering of propeller noise by the wing and other surfaces. Both justify dedicated studies, to understand, model, and optimize all aspects of propeller-airframe integration. Within this context, resorting to analytical models is an attractive approach. However, analytical modeling requires that the dominant sound-generating mechanisms are previously identified, on the one hand, and that simplifications are accepted for mathematical tractability, both on the flow features and the geometry, on the other hand. Furthermore, the models must include design parameters as realistically as possible for practical use in optimization algorithms.

Especially when analytical methods are used, the noise radiated by a propeller in free field is often predicted, relying on Ffowcs Williams & Hawking’s formulation of the acoustic analogy. The analogy states that, from the standpoint of a distant observer, the moving blades can be replaced by equivalent monopoles, dipoles, and quadrupoles [6, 7]. The latter corresponds to thickness noise, loading noise, and flow noise, respectively. The analogy equation is solved with the free-space Green’s function, either in the time domain or in the frequency domain. In installed configurations, the diffraction of propeller noise by the airframe or surrounding surfaces must be explicitly considered, because it is able to strongly restructure the sound field. In this case, the wave equation or the Helmholtz equation must be solved with additional boundary conditions imposed on the surfaces. In a general case, this is achieved with numerical methods. Alternatively, a tailored Green’s function can be used, provided that the geometry of the surfaces can be simplified, preserving the dominant scattering effects. This enables one to develop a complete analytical approach, including source modeling and diffraction. The present study aims to demonstrate the usefulness of this approach, particularly at the early design stage of a mechanical system, in the context of innovative, installed, and/or distributed propulsion systems.

In essence, the approach has to start with the definition of a generic configuration, in which a propeller and a scattering surface are arranged with variable positioning parameters. The problem is formulated in the frequency domain because diffraction is a matter of comparing dimensions and wavelengths. For mathematical tractability, in particular separation of variables and homogeneity in the expression of boundary conditions for the Helmholtz equation, the surface is defined along iso-values of the coordinate system. The surface must also be compatible with a uniform fluid motion, corresponding to forward flight. In the present work, the generic configuration includes a flat rectangular plate mimicking a wing, embedded in a mean-flow normal to its edges, and a pair of side-by-side propellers in the aft part of the wing. This configuration corresponds to a real one that will be tested as a part of the ongoing research project ENODISE. Analytical modeling is understood as a way of exploring many geometrical parameters and propeller operational conditions with a minimum cost to select either promising or detrimental configurations prior to their detailed characterization in the experiment. More precisely, the relative wing-propellers positioning is the main investigated parameter. A key aspect of being assessed is that placing the propulsion units over the wing and at a quite short distance to its surface is expected to bring the benefit of shielding for observers on the ground.

The present paper is organized as follows. The generic configuration of interest is depicted in section III. The key steps of the analytical methodology and mathematical background of the sound-scattering model are reported in section IV. The dipole sources are recognized as dominant at the low Mach numbers of interest. The free-field radiation model of propeller noise, including the estimation of the steady-loading and unsteady-loading noise sources and their expansion into source-modes, is presented. The basic sound scattering by the trailing edge is modeled, resorting to the rigid half-plane Green's function for the Helmholtz equation. An innovative and simple finite-chord correction applied to the scattering model and its numerical validation are described in section V. Finally, validation tests and main results are presented and discussed in section VI, prior to some concluding remarks.

III. Propeller-Wing Configuration

The selected propeller-wing configuration, depicted in Figure 1, includes a finite thin plate and two six-bladed side-by-side subsonic propellers of 0.2 m diameter, installed at different positions near the trailing edge. It is representative of drones or future electric distributed propulsive architectures for aircraft.

Various mechanisms are expected in such an arrangement. First, the blades interact with the wake or the potential upstream field of a pylon in the over-the-wing configurations. This induces blade-loading harmonics (BLH) on the blades and subsequent tonal noise radiation. Other BLH are produced as the blade tips cross the boundary layer or the wing's wake for some relative positions. Additionally, suppose the blade tips are close enough to the wing trailing edge. In that case, a possible amplification occurs because of the asymptotic behavior of the Green's function for compact source-to-edge distances. This effect typically regenerates sound in the shadow region for masking configurations (see subsection IV.E). If the blade tips operate outside the mean-flow gradients of the wing, diffraction of free-field propeller noise is the only remaining effect; the important question is whether the amplification operates or not. Both aerodynamic and acoustic installation effects make a significant sound increase expected as the propeller distance to the plate is reduced. However, which installation effect dominates is probably a matter of combined parameters, which must be clarified.

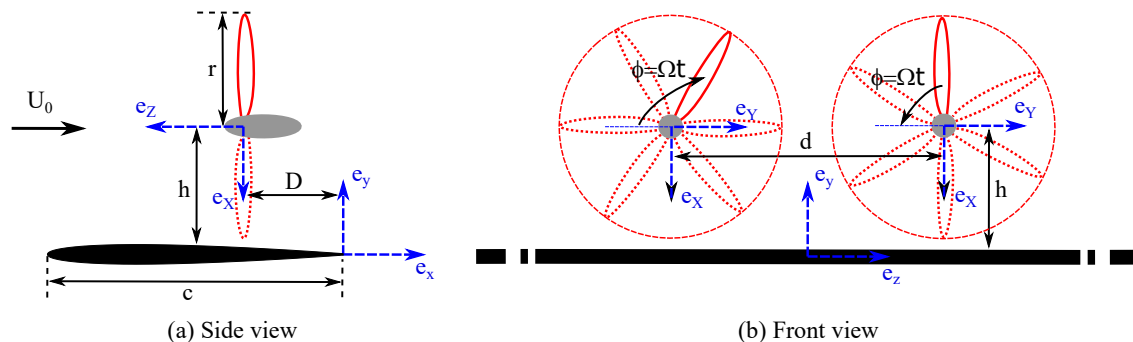


Fig. 1 Wing-propellers configuration, reference frames and main notations.

Several configurations were analytically assessed, as shown in Table 1; only the most critical cases, depicted in Figure 2, will be analyzed and discussed.

Table 1 Parametric variations of the wing-propellers configurations. r is the radius of the propellers.

	1	2	3
D	r	$0.5r$	$0.1r$
h	$r+r$	$r+0.5r$	$r+0.1r$
d	$2r+r$	$2r+0.5r$	$2r+0.1r$

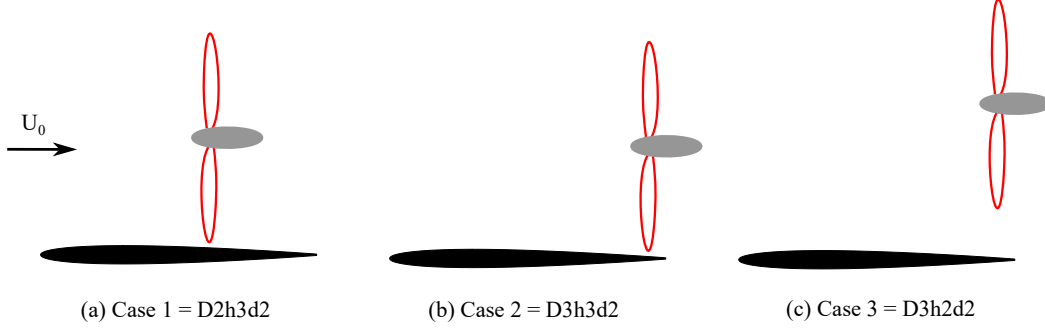


Fig. 2 Wing-propellers critical configurations. Same distance between propellers in all cases.

IV. Analytical Tonal Noise Prediction

This section first reviews the elementary expressions of the tonal noise radiated by a propeller in the far-field. They are used only as a reference for analyzing the modal properties of the radiated field. Next, the formalism of source-modes is introduced, from which the sound field could be expressed uniformly in the whole space. Such a procedure is well suited when the near-field investigation is interesting. It is also extendable to various configurations, such as a pair of synchronized propellers, and can be easily related to the physical BLH sources. Finally, the diffraction model is developed in a second step, based on the Green's function tailored to the geometry.

A. Rotating Dipole

Propeller tonal noise is radiated at multiples of the blade-passing frequency (BPF), noted $\omega/(2\pi) = mB\Omega/(2\pi)$, where Ω stands for the angular rotational frequency and B the number of blades. In free-field, the noise radiated by a propeller with the real flow corresponding to an installed configuration; thus, the true sound sources (but ignoring additional scattering) are predicted relying on Ffowcs Williams & Hawking's formulation of the acoustic analogy [6, 7], reduced to the dipole source terms. The tonal noise is formulated in the frequency domain, and the far-field is expressed in such a way suited to highlight the modulation by the azimuthal flow distortions and interference properties between blades. At the multiple of order m , and for a blade segment of mean radius r , the general expression for the far-field complex-valued sound-pressure amplitude at observer point \mathbf{x} reads as follows, with the convention $e^{-i\omega t}$ for monochromatic waves:

$$p_{mB}(\mathbf{x}) = \frac{ik_{mB}r}{4\pi} \sum_{s=-\infty}^{\infty} F_s(r) \left\{ \cos\Theta \cos\gamma(r) G_{mB-s}^{(1)} + \sin\Theta \sin\gamma(r) G_{mB-s}^{(2)} \right\} \quad (1)$$

with $k_{mB} = mB\Omega/c_0$, and

$$G_n^{(j)} = \frac{\Omega}{2\pi} \int_0^{2\pi/\Omega} G_j(t) e^{in\Omega t} dt, \quad G_1(t) = \frac{e^{ik_{mB}R'}}{R'^2} \left[1 - \frac{1}{ik_{mB}R'} \right], \quad G_2(t) = \sin(\Omega t - \phi) G_1(t)$$

The expression is valid everywhere in space, as discussed, for instance, by Roger & Moreau [8, 9]. It holds for a pure axial-flow architecture, both terms in the brackets corresponding to the axial and tangential components of the blade force, respectively. $\gamma(r)$ is the stagger angle, defined as the blade-segment inclination with respect to the rotational plane, or equivalently as the angle between the force and the axial direction. The observer location is defined by its spherical coordinates (R, Θ, ϕ) in the reference frame attached to the circular path of the segment of radius r , featured

in Figure 3, as well as the exact source-to-observer distance R' . The complex-valued factors $F_s(r)$ are the Fourier coefficients of the periodic force on the blade segment, referred to as the blade-loading harmonics (BLH).

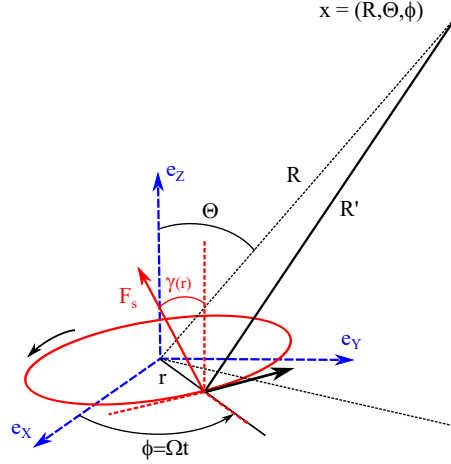


Fig. 3 Reference frame attached to a rotating blade segment and associated coordinates.

Each term of the sum defines a free-field radiation mode of order $n = mB - s$. Its radiating structure expresses the coherent character of the sound sources and the associated interference between blades. The interference is better emphasized with the acoustic and geometric far-field approximation, corresponding to $k_{mB}R' \gg 1$ and leading to the following expression:

$$p_{mB}(\mathbf{x}) = \frac{iB k_{mB}}{4\pi R} e^{i k_{mB}R} \sum_{s=-\infty}^{\infty} F_s(r) e^{i n (\phi - \pi/2)} J_n(mB M(r) \sin \Theta) \left[\cos \Theta \cos \gamma(r) - \frac{(mB - s) \sin \gamma(r)}{mB M(r)} \right] \quad (2)$$

noting that $k_{mB}r = mB M(r)$, where $M(r) = \Omega r / c_0$ is the tangential Mach number at the current radius. The order n appears as the number of azimuthal lobes of the mode.

The contribution of the near field terms is neglected in Equation 1; nonetheless, it is essential for installation-effect studies. Therefore, introducing the formalism of source-modes (see next section) as an alternative to Equation 1 is well suited to illustrate the formation of acoustic wavefronts from the near-field of distributed sources. The far-field expression, Equation 2, highlights which BLH are effectively contributing to a given BPF harmonic. Indeed, the Bessel function rapidly drops to zero as its order exceeds the value of its argument in absolute values. Thus, it operates as a 'band-pass' filter on the BLH spectrum. Furthermore, Equation 2 is used to compare predictions with measurements directly, usually carried out with far-field microphones.

B. Source-Mode expansion

According to the general rotor tonal-noise formulation, Equations 1 and 2, the sound radiated at the frequency $mB\Omega/(2\pi)$ by the array of the same element repeated on all blades is expressed as a sum of spinning radiation modes. Each isolated mode is defined by its amplitude, the number of lobes n , and azimuthal phase velocity $\Omega_s = mB\Omega/n$. Its acoustic field can be reproduced from a continuous circular distribution of stationary point dipoles of the same radius r as the true source of the mode, provided that a proper phase shift is applied to the distributed dipoles and their orientation is defined accordingly. Such a distribution is called a source mode. For the source-mode n associated with the BLH of order s , the strength of the dipole source at angle α_d on the circle and at time t is $F_t(\alpha_d, t) = F_d e^{-i mB\Omega t}$ with $F_d = F_s e^{-i n \alpha_d}$, where F_s is the BLH defining the dipole strength [10, 11]. Practical implementation is achieved by discretizing the source-mode as an array of point dipoles. For each dipole, the contribution to the sound is expressed by the scalar product of the dipole strength by the gradient of the free-space Green's function for the Helmholtz equation.

The source-mode identity could be thought of as redundancy for free-field calculations. However, it is well suited for understanding the formation of rotating-blade noise wavefronts close to the sources. Moreover, it is very convenient to model the acoustic scattering by surrounding solid surfaces of arbitrary shape. Indeed, scattering is a matter of the

relative position of a source to the surfaces and the distance-to-wavelength ratio. The total sound field can be reproduced by a linear superposition of the scattered and direct fields calculated for all stationary dipoles of a source-mode circle, as diffraction problems are usually formulated in the frequency domain for stationary sources. This can be achieved in a semi-analytical way if a tractable expression of the tailored Green's function is available (see the application in section VI). Otherwise, the source-mode identity can be combined with a numerical integral formulation of the diffraction problem [12].

C. Steady-Loading Noise Estimates

For subsonic installed rotors, steady-loading noise is most often of secondary importance compared to unsteady-loading noise because of the higher radiation efficiency of blade-loading harmonics induced by the azimuthal mean-flow distortions. Indeed, the associated rotor-locked modes, simulated by source-modes with orders equal to multiples of the blade number, produce an evanescent sound field. However, this general free-field status obviously holds in the presence of a sufficient amount of distortion and becomes questionable for small blade numbers. Moreover, the scattering by obstacles in close vicinity of the source circle, particularly by the trailing edge of a wing, can convert evanescent modes into effectively radiating patterns, leading to reconsidering the ranking. Therefore, the analysis must consider steady-loading noise and unsteady-loading noise as two competing mechanisms. For both, the same approach consists of splitting a blade into annular strips, assuming homogeneous flow conditions along with a strip's spanwise extent, for mathematical tractability. For steady-loading noise, shortly discussed in this section, this reduces to a simple implementation of the Blade-Element Momentum Theory (BEMT).

Opposite to the case of unsteady-loading noise, blade-design parameters need to be specified. This seems contradictory with a predictive approach at the early design stage when some parameters are still unknown. Therefore, a short inspection is made in this section, showing the sensitivity of steady-loading noise with the main parameters involved in the BEMT, namely the spanwise distributions of chord and twist. Two designs corresponding to identical blade numbers and overall dimensions are compared, summarized in Figure 4. Both are typical APC designs, one of which is reproduced from Romani [13]. Furthermore, the lift coefficient curve of the NACA-4412 airfoil is assumed. Though arbitrary, this choice is not believed to question the basic conclusions.

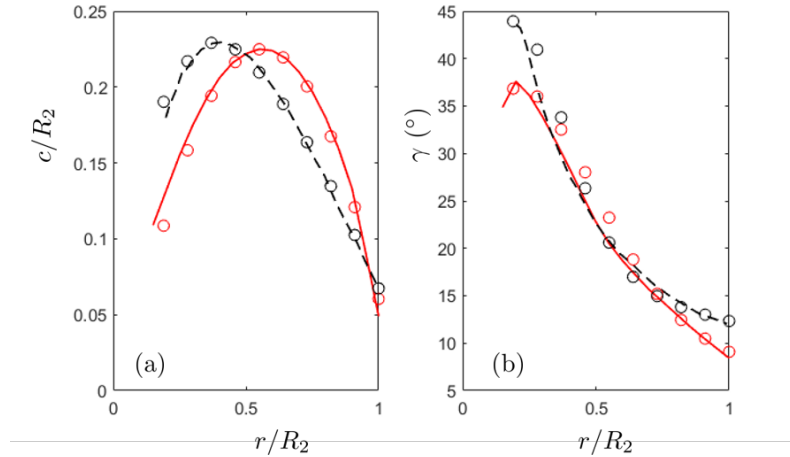


Fig. 4 Radial distributions of chord length (a) and twist (b), for two blade designs of APC types. Black-dashed lines stand for the test case reported by Romani [13].

Once a blade is split into a series of segments, the BEMT is applied for each segment, at specified rotational speed and advance ratio $J = \pi U_a / (\Omega R_2)$, where U_a denotes the flight speed, assumed parallel to the axis. The induced speed on the segment numbered j reads

$$\frac{v_i}{\Omega r_j} = \frac{1}{2} \left[-\frac{U_a}{\Omega r_j} + \sqrt{\left(\frac{U_a}{\Omega r_j}\right)^2 + \frac{B c_j}{2\pi r_j} (C_L \cos \xi - C_D \sin \xi)} \right], \quad (3)$$

and the local angle of attack α_j is defined as

$$\alpha_j = \gamma_j - \tan^{-1} \left(\frac{U_a + v_i}{\Omega r_j} \right), \quad (4)$$

if B is the number of blades and r_j is the mid-span radius of the segment. The coupled Equations 3 and 4 are solved iteratively, starting from a zero induced speed. Convergence to the values (α_j, v_j) is reached after a couple of iterations, providing the values of the lift and drag coefficients $C_L(\alpha_j)$ and $C_D(\alpha_j)$. The latter determines the axial and tangential forces needed for the sound predictions. Tests made on a configuration reported by Romani [13], not shown here, were found in a good overall agreement with both measured data and numerical simulations performed with a LBM software. This confirms that relevant steady-loading noise predictions can be obtained with the BEMT for the sake of further indicative comparison with unsteady-loading noise calculations.

Test predictions made with the two-blade designs in Figure 4 are reported in Figure 5, for $B = 2$ and a rotational speed of 5,000 rpm, as a function the advance ratio. Nearly the same thrust coefficient is achieved, with similar levels of steady-loading noise, despite the significantly different blade designs. Small discrepancies in sound pressure level are only observed at the highest advance ratios, corresponding to the lowest thrust coefficients. It can also be guessed that, as long as they correspond to only slight differences in lift coefficient at a given Reynolds number, other blade cross-section shapes would not produce large differences, at least for the same technological option or family of propellers typically here with straight blades. Tests have been repeated assuming six blades and the same rotation speed of 5,000 rpm, in which case steady-loading noise is dramatically reduced to below 30 dB at the BPF. The results are added in Figure 5-a. All blade angles have been arbitrarily increased by 5° in this second test for a more realistic operation, which leads to substantially higher thrust ratios, also added in Figure 5-b. Again, the results are found nearly insensitive to precise blade design.

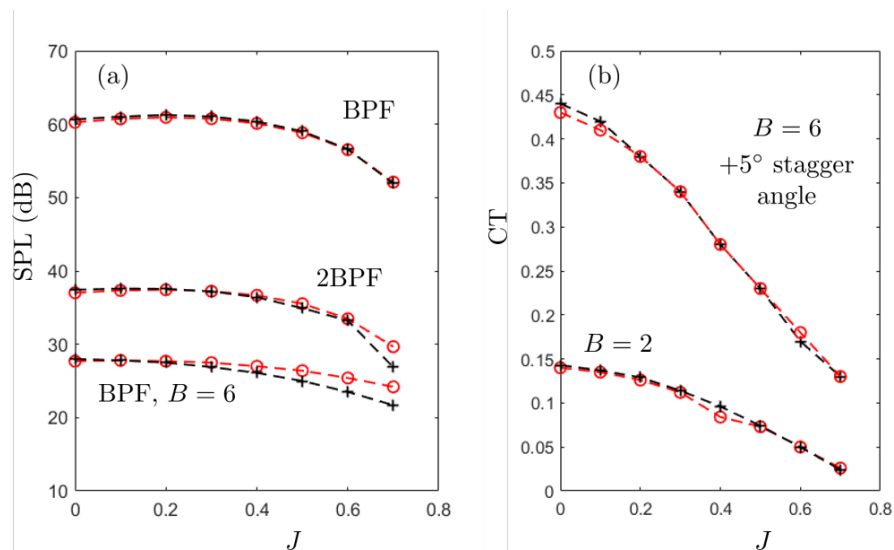


Fig. 5 (a): predicted steady-loading noise levels at the first two BPF tones for a 2-bladed propeller, and for a 6-bladed propeller at BPF, as a function of advance ratio. Tip radius 15 cm, rotational speed 5,000 rpm. (b): corresponding thrust ratios. Blade designs in Figure 4.

Within the scope of an early-design approach in which only global parameters are known, steady-loading noise appears as essentially a matter of combined Mach number and blade number and, to a lower extent, of thrust coefficient *via* the advance ratio. This makes reliable estimates possible with only a minimum knowledge of parameters. It is worth noting that the sound from steady-state aerodynamics of blades also includes thickness noise. However, for most technologies involving thin-enough blades, this noise remains lower than steady-loading noise, except in some directions of possible steady-loading noise extinction. Furthermore, both correspond to the same rotor-locked radiation modes and the same dipolar character of the equivalent sources, provided that Isom's formulation of thickness noise is used [14]. For this reason, thickness noise is not discussed in this work.

D. Unsteady-Loading Noise Sources - Wake Model and Distortion Harmonics

Installed propellers operate in stationary azimuthal distortions. This induces on the blades periodic lift fluctuations, which are the sources of unsteady-loading noise. For DEP architectures, the distortions can be the wake of the wing or of an upstream support, of the potential field of a downstream pylon. They can also be the local fluid acceleration and the boundary layer developing over the wing, periodically crossed by the blades, for an installation close enough to the wing. Other sources of unsteady loads on the blades arise from the aerodynamic coupling between propellers positioned side-by-side at short distance from each other. This variety of conditions makes unsteady-loading noise intrinsic to the installation but not to the original blade design. Furthermore, the response of the blades to variations of the relative velocity does not depend significantly on the cross-section shape, as stated by linearized unsteady-aerodynamic theories. Instead, it is usually derived, assimilating the blade segment to a zero-thickness flat plate of the same span, chord, and stagger angle. When unsteady-loading noise must be compared to steady-loading noise, one key aspect is the amplitude of the lift fluctuations compared to the mean lift. Another one is the typical angular extent of the distortion compared to the circular path of a blade segment. In this section, an indicative Gaussian wake profile applied to the axial velocity is considered as a model distortion.

At a given radius r , the Gaussian velocity deficit is defined by its depth w_0 and its characteristic half-width b_0 , assumed shorter than the perimeter $2\pi r$ followed by the blade segment for consistency. The periodic passage of the blade segment through the distortion produces a periodic upwash in a reference frame attached to the segment, the amplitude of which is defined by w_0 and by the normal projection with the factor $\cos \gamma(r)$. Either smooth or sharp distortions are obtained depending on whether the ratio $b_0/(2\pi r)$ is relatively large or small, respectively. Smaller values induce more impulsive lift variations on the blades, corresponding to efficient higher-order harmonics in the sound spectrum.

The periodicity is expressed by an infinite series of Gaussian time pulses:

$$w(t) = \bar{w}_0 \cos \gamma(r) \sum_{n=-\infty}^{\infty} e^{-\xi(t-nT)^2/\tau^2}, \quad (5)$$

where $\xi = \ln 2$, $\tau = b_0/(\Omega r)$ is the half-time of the pulse due to a single passage and T the period of rotation corresponding to the rotating frequency $\Omega/(2\pi)$. The upwash is expanded in the Fourier series

$$w(t) = \sum_{s=-\infty}^{\infty} w_s e^{-i2\pi st/T}, \quad w_s = \frac{1}{T} \int_0^T w(t) e^{i2\pi st/T} dt$$

where the complex coefficients w_s are the distortion harmonics, each of which induces a blade loading harmonic of same order F_s . They are found as

$$w_s = \frac{\Omega \bar{w}_0 \cos \gamma(r) \tau}{2\pi} \sqrt{\frac{\pi}{\xi}} e^{-(s\Omega\tau)^2/(4\xi)} \quad (6)$$

For consistent but rough estimates, the relationship between the coefficients w_s and F_s per unit span is provided by Sears' theory, as

$$F_s = \pi \rho c U_0 w_s S \left(\frac{s\Omega c}{2U_0} \right), \quad (7)$$

S standing for Sears' function and U_0 for the relative speed on the blade. For the assumed Gaussian profile, the envelope of the distortion-harmonic spectrum is also Gaussian, decreasing faster as the half-width of the distortion increases. The model is handy for analyzing wake crossing. Typically, the near wake is deeper and narrower, closely downstream of a pylon, within a quarter chord length, with relatively large values of w_0 and small values of b_0 or τ . In contrast, the opposite situation is encountered in the far wake.

For the practical inspection of an installed configuration, and if the aforementioned Gaussian model is retained, representative parameters b_0 and w_0 need to be defined first, and the amplitudes of the blade-loading harmonics F_s expressed as a percentage of the steady loading. Then Equations 1 or 2 provides compared tonal-noise estimates, corresponding to the free-field. At this stage, only the aerodynamic installation effect is accounted for. The same can be achieved for any distortion model, either defined by analytical expressions or by the numerical azimuthal Fourier series of an arbitrary field. No precise application is detailed in the paper; the aforementioned procedure is only described for methodological purpose. An example of propeller-wing wake interaction with arbitrary relative positioning is described in the reference [15]. A simple analysis of orders of magnitude, which can help anticipate some results, is now given to close the section.

For a given amplitude of the velocity fluctuations in terms of upwash w_s , the ratio of BLH to steady-loading strength is about

$$\left| \frac{F_s}{F_0} \right| \approx 2a \frac{\pi}{C_L} S \left(\frac{s \Omega c}{2 U_0} \right),$$

if C_L denotes the lift coefficient and $a = |w_s/U_0|$. For a segment of 2 cm chord at a radius of 10 cm, the modulus of Sears' function can be approximated as $[1 + 0.6s]^{-1/2}$. Assuming 5% of velocity fluctuations and a lift coefficient of order 1 leads to $|F_s/F_0| \sim 0.3 [1 + 0.6s]^{-1/2}$, which is about 0.14 at the sixth BLH, feeding the symmetric radiation mode at the BPF. Though Sears' theory is known to overestimate the blade response, this value is quite large. Now diffraction tests, not reported here, indicate that the symmetric mode is not amplified by the compact regime of the Green's function, whereas the rotor-locked mode of order 6 is substantially amplified, as shown later on in subsection VI.B. This simple remark shows how source ranking is modified in the presence of scattering surfaces.

E. Propeller Noise Scattering - Half-Plane Green's Function

For complete acoustic estimates, it is crucial to consider the diffraction of acoustic waves emitted by the propulsive system or by solid bodies located near a wing, such as landing gears and/or high-lift devices. The complicated geometry of an aircraft makes numerical tools necessary to quantify this effect accurately. However, for simpler assessment at the early design stage, analytical formulations can be preferred as alternatives at the price of crucial geometrical simplifications. In the present work, the retained dominant mechanism is the scattering of propeller noise by the wing trailing edge. For this, in a first step, the wing is mimicked by a zero-thickness rigid half-plane extending to infinity upstream and embedded in a uniform flow. This allows to use the half-plane Green's function for the convected Helmholtz equation, the problem being solved in the frequency domain. This approach has been thoroughly addressed in the aeroacoustic literature for predicting the sound scattering by trailing edges in the presence of a mean fluid motion [10, 16, 17]. Such an approach also requires that the true sound sources are described in terms of stationary sources, which is ensured by the source-mode formalism. Nevertheless, suppose these simplifications are representative of the underlying source and diffraction mechanisms. In that case, they may provide a quick estimate of the radiated sound, reliable enough to compare various installed propeller configurations. In particular, the simplifications must enable to infer orders of magnitude of the possible amount of reduction brought by a masking strategy, for instance, installing propellers just above a wing, closely upstream of the trailing edge.

Figure 6 illustrates the test configuration, involving two side-by-side contrarotating source modes, which mimic a pair of contrarotating propellers, and the half-plane accounting for the rear part of a wing. Results shown hereafter will be displayed on three planes. The first one is the streamwise plane containing the axis of the right source circle, aimed at characterizing the scattering from a lateral point of view. The second one is the front plane providing a view towards the upstream direction, introduced to assess the radiation in a plane parallel to the shifted mode circles. Both modes are spinning in the same frontal plane. The third one is a horizontal plane located below the scattering half-plane, also considered to assess the noise perceived by an observer on the ground under the flight path of an aircraft, even if the relatively moderate distance is not fully representative yet of the acoustic and geometric far-field. In addition, it provides an insight into the masking effect as a function of the source position relative to the plate.

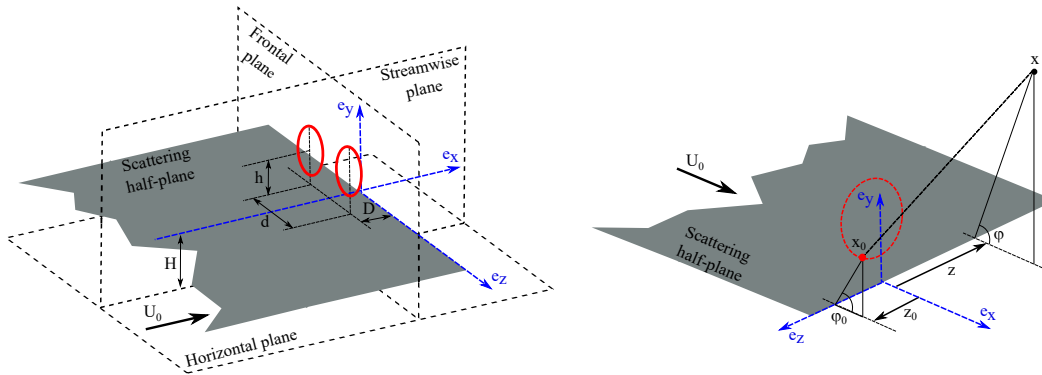


Fig. 6 General half-plane reference frame. Scattering planes and side-by-side contrarotating source modes positions (left) and notation for source and observer locations (right).

Use is made of the analytical expression of the half-plane Green's function introduced first by MacDonald [18] in a quiescent medium and readdressed by Jones [19], Rienstra [17], and Roger *et al.* [10] in two dimensional and three-dimensional forms with a uniform flow normal to the edge. Ffowcs Williams & Hall also applied this function in their far-field approximation of turbulence scattering into sound in the vicinity of trailing edge [20]. An important outcome is that some amplification operates on dipoles, with the factor $(k \varrho_0)^{-1/2}$, for sources approaching the edge [10]. This compact scattering regime corresponds to a cardioid radiation pattern. In the present investigation, the sources of propeller noise are distributed on a circle of arbitrary radius and distance to the trailing edge. If the diameter is sufficiently large with respect to the wavelength, some source positions can get very close to the edge, whereas others remain well apart, leading to some imbalance between the scattered source components of a rotor. The exact formulation of the Green's function is therefore needed.

The Green's function is valid for arbitrary positions of the sources and the observer but ignores span/chord-end effects. It provides an approximation by reproducing the main physical features for sources close enough to a trailing edge in terms of geometrical parameters and radiating at wavelengths sufficiently lower than the actual chord and span. If expressed in cylindrical coordinates for an observer at point $x = (r, \theta, z)$ and a source point $x_0 = (r_0, \theta_0, z_0)$, with the z -axis along the edge and θ being π along the half-plane and zero in its continuation Figure 6, the three-dimensional form of the half-plane Green's function in a medium at rest reads

$$G_{1/2}^{(0)}(\mathbf{x}, \mathbf{x}_0) = \frac{-ik}{4\pi^2} \left\{ \int_{-\infty}^{u_0} \frac{K_1^*(ikR\sqrt{1+u^2})}{\sqrt{1+u^2}} du + \int_{-\infty}^{u_1} \frac{K_1^*(ikR'\sqrt{1+u^2})}{\sqrt{1+u^2}} du \right\}, \quad (8)$$

where K_1^* is the complex conjugate of the modified Bessel function of order 1. $\mathbf{x}_0 = (x_0, y_0, z_0)$ and $\mathbf{x} = (x, y, z)$ are the source and observer vectors respectively and $k = \omega/c_0$. The exact acoustic pressure field of a point dipole is given by the scalar product between its strength \mathbf{F} and the gradient of the Green's function, as $P_{1/2}^{(0)} = \mathbf{F} \cdot \Delta G_{1/2}^{(0)}$. Thus Equation 8 is the basis for deriving the uniformly valid radiated field of arbitrary source distributions accounting for the diffraction by the edge, at the price of numerical treatment of the integrals and derivatives concerning the source coordinates. The dependence $e^{-i\omega t}$ of monochromatic waves is implicitly assumed. The distance variables and upper bounds of the integrals are given by the following expressions, where the subscript 0 is the notation referring to the source location:

$$u_0 = \frac{2}{R} \sqrt{rr_0} \cos \frac{\theta - \theta_0}{2} \quad u_1 = -\frac{2}{R'} \sqrt{rr_0} \cos \frac{\theta + \theta_0}{2}$$

$$R^2 = r^2 + r_0^2(z - z_0) - 2rr_0 \cos(\theta - \theta_0) \quad R'^2 = r^2 + r_0^2(z - z_0) - 2rr_0 \cos(\theta + \theta_0)$$

Flow effects associated with forward flight can be included in the scattering model by considering a uniform mean flow of Mach number M_0 , keeping the reference frame attached to the half-plane. The Green's function accounting for the presence of a uniform flow normal to the spanwise direction is obtained from the corresponding Green's function in a quiescent fluid by a Lorentz transform and stretching the space variables and by multiplying by the factor $\frac{1}{\beta} e^{iKM_0(x-x_0)}$. The rigid half-plane Green's function in the presence of a uniform flow in the positive x -direction reads:

$$G_{1/2}^{(M_0)}(\mathbf{x}, \mathbf{x}_0) = \frac{1}{\beta} e^{iKM_0(x-x_0)} G_{1/2}^{(0)}(\mathbf{X}, \mathbf{X}_0), \quad (9)$$

in which \mathbf{X} and \mathbf{X}_0 are coordinate vectors for which the streamwise coordinate x has been replaced by $X = x/\beta$, the wavenumber being rescaled as $K = k/\beta$ with $\beta^2 = 1 - M_0^2$. The flow direction is in the coordinate x to fit with the scattering by the trailing edge. The angles θ and θ_0 are defined as the corrected angles from the wake direction $x > 0$. The stretching of coordinates generates the following transformed variables:

$$\bar{r} = \sqrt{X^2 + y^2}, \quad X = \bar{r} \cos \bar{\theta} \quad \text{and} \quad y = \bar{r} \sin \bar{\theta}$$

V. Finite-Chord Correction

In the current approach of simplified geometry, considering the finite chord length c of the wing in the analysis requires replacing the rigid half-plane with an infinite strip of coordinates $(-c \leq x \leq 0, -\infty \leq z \leq \infty)$. The scattering of a source-mode by the strip may strongly differ from the ideal trailing-edge scattering deduced from the half-plane Green's function, especially if the chord length c is not much larger than the acoustic wavelength λ . Sound is scattered

by both the leading edge and the trailing edge, so that more sound is expectedly regenerated in what would be the shadow region, if any, with significant interference between sounds coming from both edges. The interference is also incomplete in the reflection region. Such effects must be accounted for when searching for some optimized configurations, which would require the exact Green's function for a strip of an arbitrary chord. Unfortunately, no uniformly-valid, closed-form expression for this Green's function is available knowledge of the authors.

High-frequency solutions for the diffraction of an acoustic plane wave by an infinite rigid strip in a fluid at rest, derived with a two-step application of the Wiener-Hopf technique, are reported, for instance, by Noble [21]. For this, two complementary half-plane problems are solved iteratively, the scattering by the second edge being understood as a correction to the scattering by the first edge. However, the two-step approach is a high-frequency approximation, typically valid for non-compact chords, that is, high values of kc . Higher-order iterations should be determined for moderate values of kc . Moreover, the plane-wave assumption is restrictive. Howe has derived a Green's function for a strip, in the case of low Mach numbers and sources close to an edge [22], using an iterative procedure and a matching with a compact Green's function for low frequencies. These reference solutions only address limited cases.

The uniformly valid formalism needed for the present investigation is missing. Therefore, a somewhat empirical correction procedure is proposed in the next section as an alternative. Its validity is assessed in subsection V.A.

A. Analytical Approximation

The aim is to reproduce finite chord effects with only minor modifications to the approach detailed in the previous section, yielding estimates of the leading edge scattering rather than exact predictions. This will allow addressing issues such as selecting suitable candidates for the propeller position and sorting out poor configurations in an optimization strategy.

The idea, illustrated in Figure 7, can be summarized as follows. In the first step, the total sound from the source-mode is calculated with the half-plane Green's function, but for the observer, locations are distributed over the finite-chord strip. For this, the observer point \mathbf{x} is approached to the surface $y = 0$ from any side. The source-mode defines the primary sources, the total sound field of which includes the direct field and the scattered field. The latter is obtained by subtracting the former from the total field. According to Green's formalism, the scattered field is exactly the direct field of secondary dipole sources distributed over the strip. After subtracting the direct field, the strength of these dipoles per unit area equals the acoustic pressure jump between both sides of the strip, which is equivalent to considering twice the scattered sound pressure at the wall $y = 0^+$. Once the secondary sources are known, their radiation is calculated in a second step with the free-field Green's function and combined with the direct field of the primary sources, which finally provides a modified total field, an 'incomplete half-plane scattering', hopefully, more reliable. Though the final combination of primary and secondary sources is fully relevant, the secondary sources are only approximate since they are deduced from a Green's function tailored to the half-plane but not to the strip.

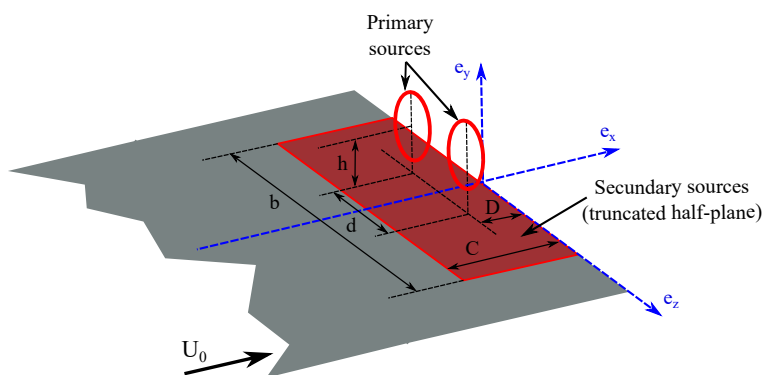


Fig. 7 Reference frame attached to a rotating blade segment and associated coordinates.

Furthermore, the strip must also be truncated spanwise for the practical implementation, with some span length L . This effect is not addressed in the present model. However, a dimensional argument suggests that a finite span would not significantly modify the radiation for $L/\lambda \geq 1$ and for observation angles that are not too shallow in the spanwise direction.

B. Numerical Validation

In order to assess the accuracy of the proposed analytical approximation, a comparison is made in this work with a numerical simulation. The comparison is performed in a two-dimensional case, including a finite-chord segment or a true airfoil shape, and a point dipole source, in the presence of a uniform mean flow. The numerical model solves the convected Helmholtz equation using a p -adaptive finite element method [23]. In this approach, an *a-priori* error indicator is used to adjust the order automatically in the elements to maintain a target accuracy, accounting for the local mesh size, frequency, mean flow magnitude, and direction [24]. In this study, all computations were performed using an engineering target accuracy of $E_t = 0.1\%$. The finite element unstructured mesh is generated using Gmsh [25]. An automatic Perfectly Matched Layer is applied on the outer boundaries in order to efficiently absorb the outgoing waves [26]. The dipole source is implemented as a right-hand side in the convected Helmholtz formulation. Note that a uniform mean flow is considered, including the true airfoil shape. A subsequent paper will examine the influence of the mean flow variations around the non-zero thickness airfoil.

VI. Results

A. Validation of the Green's Function Approximation

The relevance of the analytical approximation is assessed in this section by comparing it with the numerical approach of subsection V.B. The test, reported in Figure 8 as instantaneous sound-pressure maps, is made with a 2D reduction of the formalism. A point dipole is placed at some short distance of a finite plate of chord lengths $c = \lambda$ (Figure 8-a,b) and $c = \lambda/2$ (Figure 8-c,d).

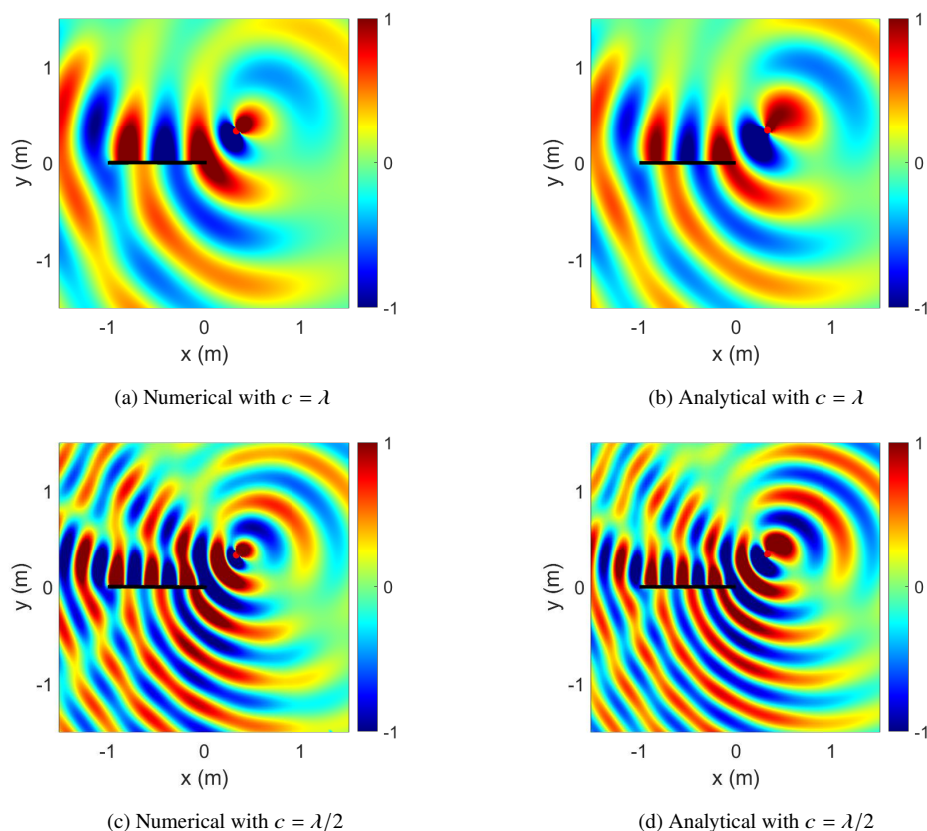


Fig. 8 2D numerical and analytical instantaneous sound-pressure maps of a dipole in the presence of a finite-chord plate. The dipole is featured by the red dot and the finite plate is shown in black. Same arbitrary color scale on all plots.

Very similar wavefront patterns are found. The test corresponds to a main lobe of the direct field from the

source, impinging on the trailing edge. This condition is known as responsible for the significant regeneration of sound in the geometrical shadow region. In fact, for both frequencies, there is no masking by the plate but rather a wavefront restructuring with multiple directivity lobes. The analytical approximation is found to reproduce these features realistically.

For a more quantitative assessment, Figure 9 and Figure 10 display compared sound-pressure profiles extracted along a horizontal line just above the flat-plate and a vertical line at the end of the flat-plate, featured by the red dots in the figures. Discrepancies remain very acceptable with regards to noise estimates in terms of decibels. This confirms the validity of the truncation procedure introduced in section V.

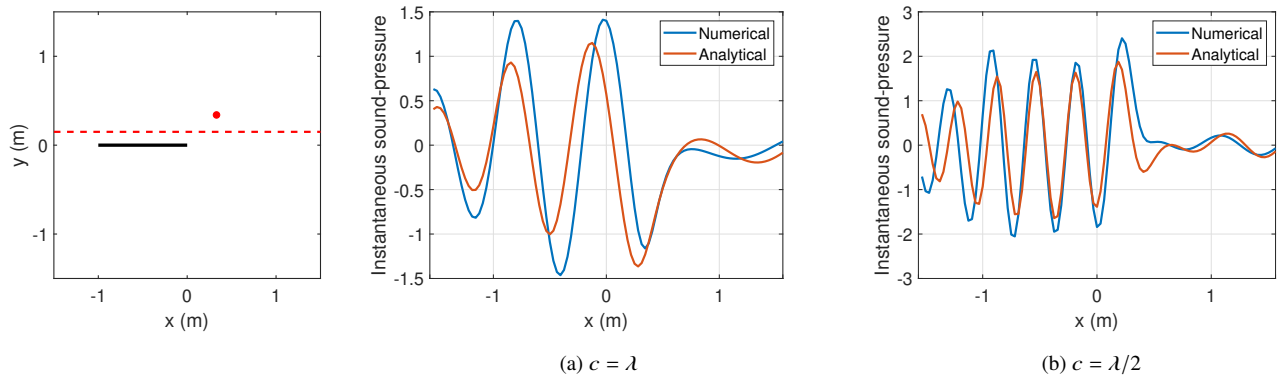


Fig. 9 Horizontal line comparison between numerical and analytical instantaneous sound-pressure maps of a dipole in the presence of a finite-chord plate.

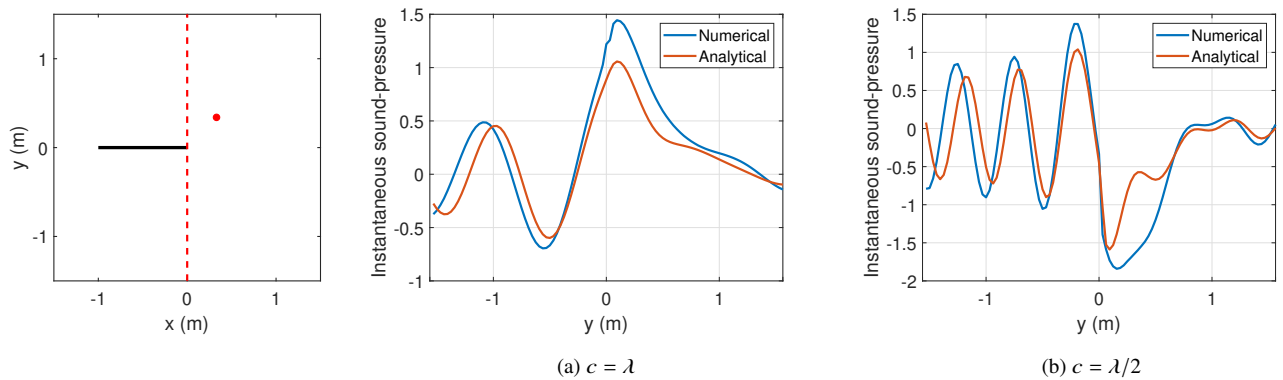


Fig. 10 Vertical line comparison between numerical and analytical instantaneous sound-pressure maps of a dipole in the presence of a finite-chord plate.

Figure 11 shows further computed sound-pressure maps of a dipole source in the presence of a NACA-0012 airfoil. In this case, the simulated wave-front patterns are similar to those with the flat-plate, in Figure 8-a,c. Despite the significant thickness at the rounded leading edge, the precise airfoil shape has a weak effect on the sound radiation. This is attributed to the fact that, for the considered source position, the key scattering features are imposed by the trailing edge, which is 'sharp' in both cases, therefore with the same degree of singularity. Different conclusions could be drawn for sources close to the leading-edge; this aspect has not been considered in the present work. By the way, the result suggests that, at least for sources in the rear part of an airfoil or wing and for the investigated values of the chord-to-wavelength ratio, the main sound features are a matter of this ratio and source positioning. Therefore, the true shape of the airfoil can be ignored for a first insight into the scattering mechanism. Finally, the analytical model appears as a good candidate for fast and repeated calculations within the scope of parametric studies or optimization algorithms. It will be used with confidence for subsequent three-dimensional inspection of the wing-propellers configuration.

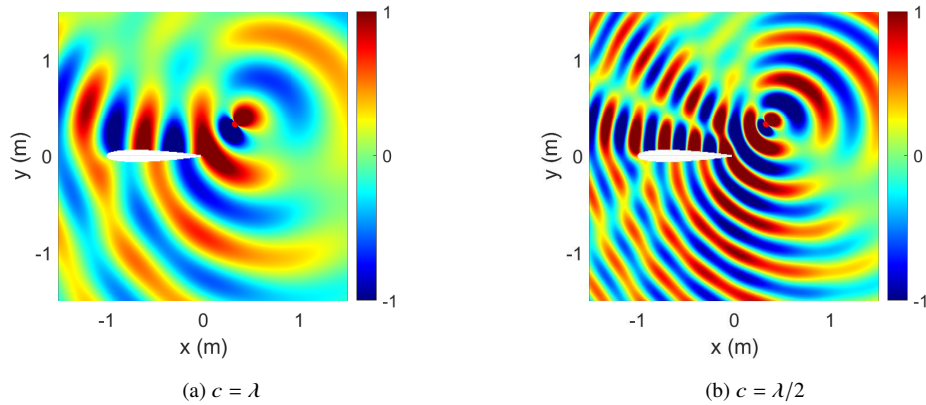


Fig. 11 2D numerical instantaneous sound-pressure maps of a dipole in the presence of the NACA 0012 airfoil. The dipole is featured by the red dot and the airfoil is shown in white. Same arbitrary color scale on all plots.

B. Wing-Propellers Test-Case Results

The results of the test cases defined in section III are presented and discussed in the present section. They complement a previous study performed with a single propeller [15]. Near-field sound-pressure maps for the rotor-locked mode $n = B = 6$, associated with steady-loading noise at the BPF, are shown in Figure 12, in complementary perpendicular planes, namely the propeller plane $x = 0$ (a), the meridian plane $z = 0$ (b) and the wing plane $y = 0$ (c). This mode only generates an evanescent wave in free field because of the low tangential phase Mach number, which is a typical property of low Mach number propellers with significant blade numbers (see subsection IV.C).

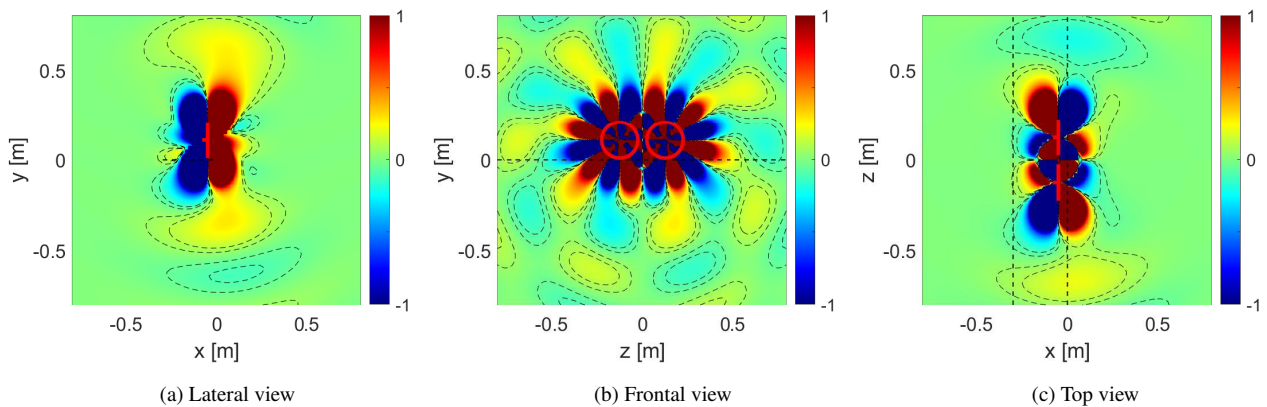


Fig. 12 Instantaneous free-field sound-pressure maps for the cumulative steady-loading noise sources (spanwise-distributed mode $n = 6$). Same color scale on all plots and iso-contours over 10% of the maximum range. Propellers featured by red circles and segments, and future wing position featured by dashed black lines.

Figures 13, 14 and 15 compare maps for the mode 6 of steady-loading noise at the BPF, in the three selected installed configurations for the same three aforementioned planes, respectively.

Significant amplification is found in all cases. The radiation is strongly enhanced in the presence of the wing because of the vicinity of the scattering edge. This is attributed to the dipole nature of the blade forces acting as sound, especially in case 1, where the blade-tip to trailing-edge distance is smaller than in the other cases. In addition, the sound regeneration effect is seen in Case 2, even though it is located at the same blade-tip to trailing-edge distance as Case 3. In case 3, the edge enters the angular range of local near-field extinction, whereas in cases 1 and 2, it enters a near-field lobe; this stresses the high sensitivity of the amplification mechanism.

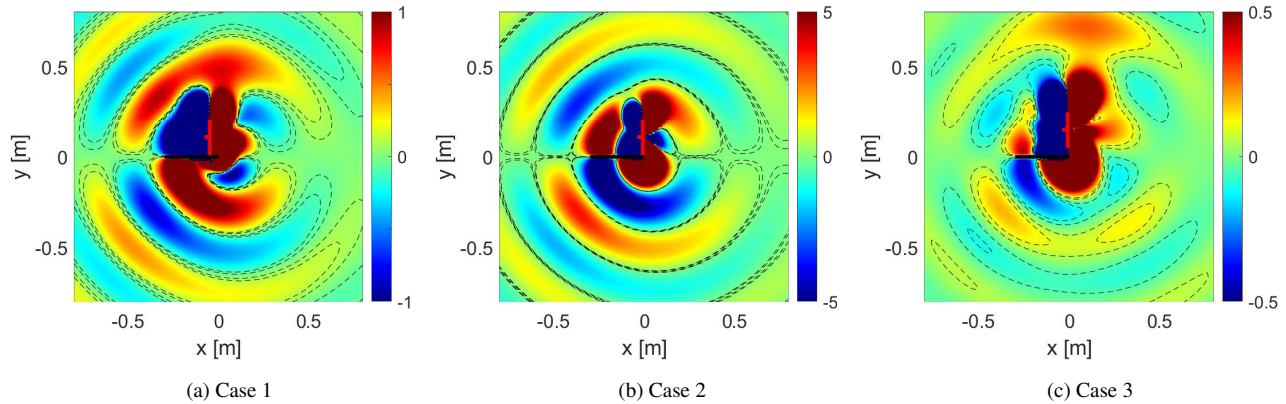


Fig. 13 Instantaneous installed-field sound-pressure maps for the cumulative steady-loading noise sources (distributed mode $n = 6$) for different cases in lateral view. Different color scale on all plots and iso-contours over 10% of the maximum range. Propellers and wing featured by red segments and black lines, respectively.

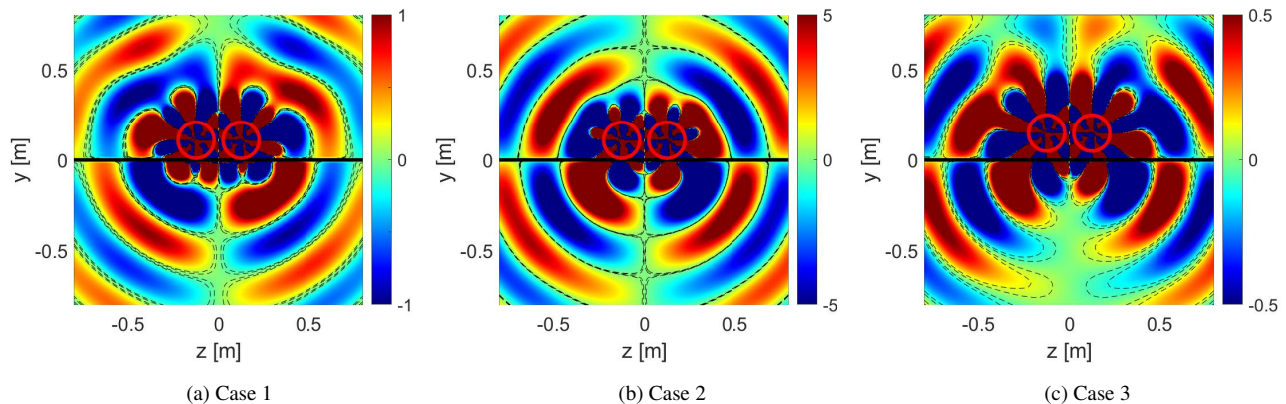


Fig. 14 Instantaneous installed-field sound-pressure maps for the cumulative steady-loading noise sources (distributed mode $n = 6$) for different cases in frontal view. Different color scale on all plots and iso-contours over 10% of the maximum range. Propellers and wing featured by red circles and black lines, respectively.

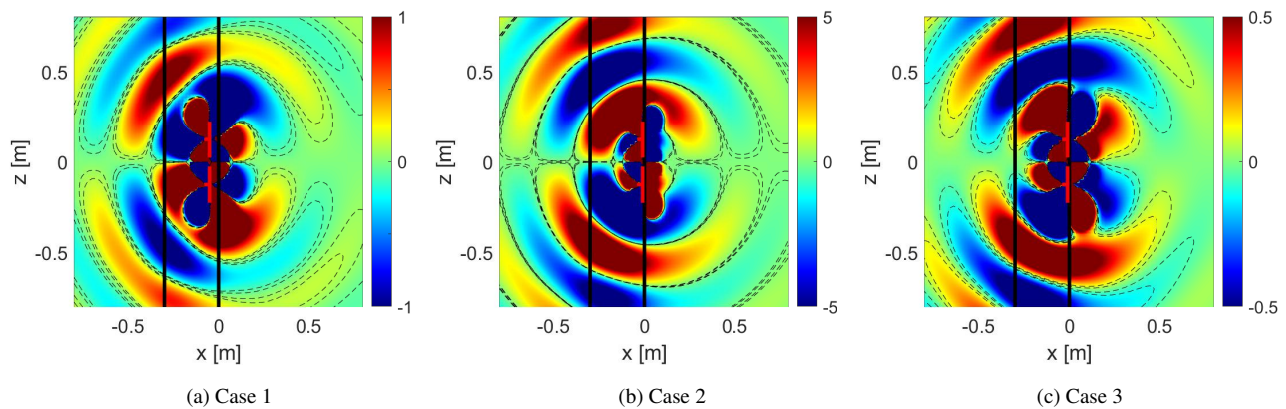


Fig. 15 Instantaneous installed-field sound-pressure maps for the cumulative steady-loading noise sources (distributed mode $n = 6$) for different cases in top view. Different color scale on all plots and iso-contours over 10% of the maximum range. Propellers and wing featured by red segments and black lines, respectively.

In addition, the scattered field features large lobes, characteristic of an equivalent lift dipole. In these cases, the distance of a part of the blade-tip circular path to the edge is much smaller than the wavelength, leading to a theoretical condition for amplification according to subsection IV.E. This suggests that for installed subsonic propellers, the steady-state aerodynamics of the blades possibly radiates loud sound, whereas it is relatively ineffective in ideal free-field conditions.

VII. Concluding Remarks

The present work combined various analytical models to investigate fundamental features of the tonal noise radiated by propellers installed on a rectangular wing. The focus was on relatively low frequencies, typically first multiples of the blade-passing frequency, representative of drones or future distributed electric propulsion architectures. This technological context implies blades operating close to the rear part of the wing, possibly including interaction with a wake-like distortion. A two-step analytical prediction method has been proposed. The first step is the calculation of the free field from the blade forces, based on a blade segmentation technique. Steady-loading noise and unsteady-loading noise sources are estimated from the blade-element momentum theory and from linearized unsteady-aerodynamic theories, respectively, for each segment. The second step is the calculation of the sound scattering by the trailing edge of the wing, starting from the exact half-plane Green's function for the convected Helmholtz equation in a uniformly moving fluid. For this, an approximate finite-chord correction to the Green's function has been proposed. In view of its partially empirical character, the approximation has been assessed against numerical simulations performed with a FEM software. The analytical and numerical predictions in the case of a zero-thickness flat plate were found in good agreement. Furthermore, the FEM simulations exhibited small differences between a flat plate and a true airfoil shape of 12% thickness for sources close to the trailing edge. This makes the analytical model an attractive and reliable tool for fast and repeated calculations in an optimization process, as long as variations in terms of decibels are considered. The coupling of sound generation and scattering models is made by replacing the true, rotating sources by equivalent circular distributions of stationary phased dipoles, called source-modes. A key outcome is that modes which would be evanescent in free field can be converted into very effectively radiating patterns if the blade tips of the installed propellers are at a compact distance from the wing trailing-edge. In particular, steady-loading noise involving rotor-locked modes enters this category. This detrimental effect of installing propellers over a wing could balance some other beneficial ones in future distributed propulsion systems. Indeed, for instance, wing-propeller vicinity possibly reduces drag by compensating the velocity deficit in the wake or in the boundary layers. Moreover, an over-the-wing installation makes some masking expected for noise exposure on the ground. The present results suggest that the amplification by compact scattering leads to reconsidering the competition between steady-loading and unsteady-loading noise contributions. The analytical tools presented in the paper are believed to be a very efficient way of quantifying these combined effects at the early design stage.

Acknowledgments

The ENODISE project has received funding from the European Union's Horizon 2020 research and innovation programme under grant agreement N°860103. The authors would like to acknowledge the Fluid Mechanics and Acoustics Laboratory (LMFA) of the department of Fluid Mechanics, Acoustics and Energetics (MFAE) from the Central School of Lyon (ECL) for providing the necessary infrastructure for the development of the research. This work was performed within the framework of the LABEX CeLyA (ANR-10-LABX-0060) of the University of Lyon.

References

- [1] ICAO, I. C. A. O., "Environmental report 2019: Aviation and Environment," *Technical report*, 2019.
- [2] Terekhov, I., "Assessing noise effects of the urban air transportation system," *2018 AIAA/CEAS Aeroacoustics Conference*, 2018, p. 2954.
- [3] Bauer, M., "FIRST ASSESSMENT OF COMMUNITY NOISE FOR A SIMULATED SCENARIO OF NEW URBAN AIR TRAFFIC," *International Congress on Sound and Vibration (ICSV), Montréal (Canada)*, 2019, pp. 7–11.
- [4] Casalino, D., van der Velden, W. C., and Romani, G., "Community noise of urban air transportation vehicles," *AIAA Scitech 2019 Forum*, 2019, p. 1834.

- [5] Bulusu, V., Polishchuk, V., and Sedov, L., “Noise Estimation for future large-scale small UAS Operations,” *INTER-NOISE and NOISE-CON Congress and Conference Proceedings*, Vol. 254, Institute of Noise Control Engineering, 2017, pp. 864–871.
- [6] Ffowcs Williams, J. E., and Hawkings, D. L., “Theory relating to the noise of rotating machinery,” *Journal of Sound and Vibration*, Vol. 10, No. 1, 1969, pp. 10–21.
- [7] Ffowcs Williams, J. E., and Hawkings, D. L., “Sound generation by turbulence and surfaces in arbitrary motion,” *Philosophical Transactions of the Royal Society of London. Series A, Mathematical and Physical Sciences*, Vol. 264, No. 1151, 1969, pp. 321–342.
- [8] Roger, M., and Moreau, S., “Aeroacoustic Installation Effects in Cooling Fan Systems Part 1: Scattering by Surrounding Surfaces,” *Proceedings of the International Symposium on Transport Phenomena and Dynamics of Rotating Machinery, Honolulu, HI, USA*, 2008, pp. 17–22.
- [9] Roger, M., and Moreau, S., “Tonal-Noise Assessment of Quadrotor-Type UAV Using Source-Mode Expansions,” *Acoustics*, Vol. 2, Multidisciplinary Digital Publishing Institute, 2020, pp. 674–690.
- [10] Roger, M., Moreau, S., and Kucukcoskun, K., “On sound scattering by rigid edges and wedges in a flow, with applications to high-lift device aeroacoustics,” *Journal of Sound and Vibration*, Vol. 362, 2016, pp. 252–275.
- [11] Roger, M., “On combined propeller synchronization and edge scattering for the noise reduction of distributed propulsion systems,” *Proceedings of the 26th International Congress on Sound and Vibration, Montreal, Canada*, 2019, pp. 7–11.
- [12] Roger, M., and Kucukcoskun, K., “Near-and-far field modeling of advanced tail-rotor noise using source-mode expansions,” *Journal of Sound and Vibration*, Vol. 453, 2019, pp. 328–354.
- [13] Romani, G., “Computational Aeroacoustics of Rotor Noise in Novel Aircraft Configurations,” Ph.D. thesis, Delft, TU Delft, 2022.
- [14] Farassat, F., “The derivation of a thickness noise formula for the far-field by Isom,” *J.Sound & Vib.*, Vol. 64, 1979, pp. 159–160.
- [15] Roger, M., Acevedo Giraldo, D., and Jacob, M., “Acoustic Versus Aerodynamic Installation Effects on a Generic Propeller-Driven Flying Architecture,” *Int. J. of Aeroacoustics*, 2022.
- [16] Jones, D. S., “Acoustic and electromagnetic waves,” *Oxford/New York*, 1986.
- [17] Rienstra, S. W., “Sound diffraction at a trailing edge,” *Journal of Fluid Mechanics*, Vol. 108, 1981, pp. 443–460.
- [18] Macdonald, H., “A class of diffraction problems,” *Proceedings of the London Mathematical Society*, Vol. 2, No. 1, 1915, pp. 410–427.
- [19] Jones, D. S., “Aerodynamic sound due to a source near a half-plane,” *IMA Journal of Applied Mathematics*, Vol. 9, No. 1, 1972, pp. 114–122.
- [20] Ffowcs Williams, J. E., and Hall, L. H., “Aerodynamic sound generation by turbulent flow in the vicinity of a scattering half plane,” *J. Fluid Mech.*, Vol. 40, No. 4, 1970, pp. 657–670.
- [21] Noble, B., *Methods based on the Wiener-Hopf technique for the solution of partial differential equations*, Vol. 332, Taylor & Francis US, 1958.
- [22] Howe, M. S., “Edge-source acoustic Green’s function for an airfoil of arbitrary chord, with application to trailing-edge noise,” *Quarterly Journal of Mechanics and Applied Mathematics*, Vol. 54, No. 1, 2001, pp. 139–155.
- [23] Bériot, H., Prinn, A., and Gabard, G., “Efficient implementation of high-order finite elements for Helmholtz problems,” *International Journal for Numerical Methods in Engineering*, Vol. 106, No. 3, 2016, pp. 213–240. <https://doi.org/https://doi.org/10.1002/nme.5172>, URL <https://onlinelibrary.wiley.com/doi/abs/10.1002/nme.5172>.
- [24] Bériot, H., and Gabard, G., “Anisotropic adaptivity of the p-FEM for time-harmonic acoustic wave propagation,” *Journal of Computational Physics*, Vol. 378, 2019, pp. 234–256.
- [25] Geuzaine, C., and Remacle, J.-F., “Gmsh: A 3-D finite element mesh generator with built-in pre-and post-processing facilities,” *International journal for numerical methods in engineering*, Vol. 79, No. 11, 2009, pp. 1309–1331.
- [26] Bériot, H., and Modave, A., “An automatic perfectly matched layer for acoustic finite element simulations in convex domains of general shape,” *International Journal for Numerical Methods in Engineering*, Vol. 122, No. 5, 2021, pp. 1239–1261.